Published in final edited form as:
J Mol Microbiol Biotechnol. 2013 ; 23(0): . doi:10.1159/000351340.

Gas vesicles across kingdoms: a comparative solid state NMR study

Eugenio Daviso[1,2], **Marina Belenky**[1], **Robert G. Griffin**[2], and **Judith Herzfeld**[1,*]

[1]Department of Chemistry, Brandeis University, Waltham, Massachusetts, USA, 02454-9110

[2]Francis Bitter Magnet Laboratory and Department of Chemistry, Massachusetts Institute of Technology, Cambridge, Massachusetts, USA, 02139

Abstract

The buoyancy organelles of aquatic microorganisms have to meet stringent specifications: allowing gases to equilibrate freely across the proteinaceous shell, preventing the condensation of water vapor inside the hollow cavity, and resisting collapse under hydrostatic pressures that vary with column depth. These properties are provided by the 7–8 kDa gas vesicle protein A (GvpA), repeats of which form all but small, specialized portions of the shell. Magic angle spinning NMR is uniquely capable of providing high resolution information on the fold and assembly of GvpA. Here we compare results for the gas vesicles of the haloarchae *Halobacterium salinarum* with those obtained previously for the cyanobacterium *Anabaena flos-aquae*. The data suggest that the two organisms follow similar strategies for avoiding water condensation. On the other hand, in its relatively shallow habitat, *H. salinarum* is able to avoid collapse with a less costly GvpA fold than is adopted by *A. flos-aquae*.

Keywords

cyanobacteria; Anabaena; haloarchaea; Halobacterium; GvpA; amyloid; supramolecular assembly; protein structure; chemical shift assignment

Introduction

A wide range of microorganisms deploy gas vesicles to regulate their buoyancy. These include over 150 species in at least five phyla of bacteria and two phyla of archaea [Walsby, 1994]. The hollow organelles are most commonly found in aquatic microorganisms. However, gas-vesicles have been observed in a soil organism [Omelchenko et al., 1993] and in an enterobacterium [Ramsay et al., 2011], where their purpose is less obvious.

The most thoroughly studied gas vesicles are those of the cyanobacterium *Anabaena flos-aquae* and the haloarchaea *Halobacterium salinarum* and *Haloferax mediterranei*, and the properties shared across these two domains are quite remarkable. Although the entirely proteinaceous shells are only 20Å thick on average [Blaurock and Walsby, 1976; Blaurock and Wober, 1976], they resist collapse. And while the gaseous contents equilibrate with the surroundings [Walsby, 1969, 1982; Walsby et al., 1992; Walsby and Simpson, 1984], water does not condense inside.

*Corresponding author: Judith Herzfeld, Department of Chemistry, Brandeis University, 415 South Street, Waltham, MA 02454-9110, USA, voice: 781-736-2538, fax: 781-736-2516, herzfeld@brandeis.edu.

The vesicle shells remain intact on washing with urea or detergent and these stripped bodies are constructed almost exclusively of the 7–8 kDa gas vesicle protein A (GvpA) [Walsby and Hayes, 1988] which is not cross-linked or otherwise post-translationally modified [Belenky et al., 2004]. The arrangement of GvpA in a low-pitch helix [Offner et al., 1998] lends the vesicles a ribbed appearance with a 46Å spacing between the ribs [Blaurock and Walsby, 1976; Blaurock and Wober, 1976] (see fig. 1). And observations of prominent x-ray reflections with 4.7Å Bragg spacings [Blaurock and Walsby, 1976; Blaurock and Wober, 1976] suggest extended β-sheet structures that could account for the amyloid-like insolubility of the vesicles [Bayro et al., 2012].

Given these shared properties, it is not surprising that the GvpA sequences are highly homologous (as illustrated in fig. 2) [Sivertsen et al., 2009; Walker et al., 1984]. Furthermore, given the unusual properties of gas vesicles, it is not surprising that GvpA's share little homology with other proteins [Ezzeldin et al., 2012; Strunk et al., 2011].

However, gas vesicles from different species also differ in some significant ways. For example, while GvpA carries a net negative charge in both *A. flos-aquae* and *H. salinarum*, this charge is much greater in the species adapted to high ionic strength environments than in the fresh water organism (see fig. 2). More vividly, species that inhabit deep waters, like *A. flos-aquae*, build narrower shells, with considerably higher collapse pressures, than species that inhabit shallow waters, like *H. salinarum* (see Figure 1). It is thought that the surface-to-volume ratio is the main determinant of the strength of the stripped shells. However, it has been proposed that the orientation of the β-sheets also plays a role. X-ray studies of aligned *A. flos-aquae* vesicles showed that the β-strands are oriented at 36° relative to the vesicle axis [Blaurock and Walsby, 1976]. Where they are sufficiently exposed along the ribs, this orientation of the β-strands has been confirmed by atomic force microscopy [McMaster et al., 1996]. It follows that the hydrogen bonds in the β-sheets must be inclined 54° from the vesicle axis, a "magic angle" that is thought to lend extra strength to the assembly [Walsby, 1994]. The corresponding information is not available for *H. salinarum* vesicles because they do not have a sufficiently large aspect ratio to be aligned easily.

Low resolution structural information, such as that described above, was all that was available for gas vesicles until recently. The large difference in electron density between the gaseous interior of the vesicles and the aqueous exterior results in multiple scattering that frustrates high resolution electron microscopy. And the insolubility of the vesicles in all but highly protic, irreversibly denaturing solvents precludes the application of solution NMR or crystallography. However, significant inroads have recently been made with magic angle spinning (MAS) solid state nuclear magnetic resonance (NMR) applied to intact (though collapsed) vesicles of *A. flos-aquae*. The significant findings are

1. general agreement with the central α-β-β-α secondary structure predicted from the primary sequence (see fig. 3) [Sivertsen et al., 2010],
2. polymorphism of the GvpA, such that the building block of the vesicles is an asymmetric dimer in which the odd-membered β-turn is shifted by one residue between the two monomers [Bayro et al., 2012; Sivertsen et al., 2009], and
3. the ribs of the vesicle are formed by a continuous cross-β ribbon that winds around the axis of the vesicle [Bayro et al., 2012].

The polymorphism is critical because it explains how the strands in the β-sheet can be oriented at 36° to the vesicle axis without situating polar residues at the interior (putatively highly hydrophobic) surface of the shell or incurring significant electrostatic penalties in the arrangement of oppositely charged residues [Sivertsen et al., 2009].

The question that we now ask, with further MAS NMR studies, is whether these detailed properties of *A. flos-aquae* vesicles are shared by the gas vesicles of *H. salinarum*. On the one hand, we might expect that they would be, given the similar secondary structure predictions (see Figure 3). On the other hand, the *H. salinarum* vesicles are not built to withstand the pressures that are experienced by *A. flos-aquae*.

Results

Dynamics

Fig. 4 shows that the dynamics of GvpA in *H. salinarum* are similar to those observed in *A. flos-aquae* [Sivertsen et al., 2010]. The relatively small cross-polarization enhancement (fig. 4a) over direct polarization (fig. 4b) indicates considerable mobility in the protein. However, only saturated groups (0 – 80 ppm) are sufficiently mobile to be detected by INEPT (fig. 4c).

Polymorphism

The first indication of dimorphism in the GvpA of *A. flos-aquae* was excess resonances in distinctive regions of the NMR spectrum. GvpA of *A. flos-aquae* has 3 glycine residues and 11 alanine residues. However, more than 3 glycine resonances and more than 11 alanine resonances appear in 2D correlations spectra [Sivertsen et al., 2009]. In contrast, although GvpA of *H. salinarum* has more glycine and alanine residues (4 and 14, respectively), the glycine and alanine regions of the ^{13}C-^{13}C correlations spectra are simpler, with no evidence of extra, distinct signals (figs. 5 and 6). Thus, in contrast to the case in *A. flos-aquae*, there is no evidence for dimorphism in *H. salinarum*. Although there remain other reasons to think that the building block of the gas vesicle is a dimer in the case of *H. salinarum* (see discussion), there is no reason to think that the dimer is asymmetric.

Chemical Shift Assignments

Sequential assignments were based primarily on a ZF-TEDOR-DARR ^{15}N-^{13}C-^{13}C spectrum [Daviso et al., 2013], representative slices of which are shown in figs. 7 and 8. The third dimension helps to separate and resolve peaks that overlap in the two-dimensional spectra.

The use of ZF-TEDOR in the first mixing step simultaneously couples a backbone ^{15}N with the ^{13}CA of the same residue and the ^{13}CO of the previous residue. This is illustrated in fig. 7, in which the slice of the spectrum corresponding to the ^{15}N chemical shift of the V47 amide shows correlation with V47CA and S46CO. It is also illustrated in fig. 8 by the appearance of the CA-CO and CO-CA correlations of residue *i* at self-consistent chemical shifts in the slices of the spectrum corresponding to the ^{15}N amide signals of residues *i* and *i +1*, respectively.

Assignments are further facilitated by a long DARR mixing period for the ^{13}C-^{13}C recoupling, which transfers magnetization along the side-chains to carbons with characteristic chemical shifts. This is illustrated in fig. 7 by the correlation of ^{13}C signals from the V47 methyl groups with the ^{15}N and ^{13}C signals from the rest of V47, and in fig. 8c by the correlation of ^{13}C signals from the F50 aromatic ring with the ^{15}N and ^{13}C signals from the rest of F50.

In total, the backbone atoms (and some, if not all, of the side-chain atoms) have been assigned for 52 of the 75 residues in GvpA. While most of the highly conserved region (see fig. 2) has been assigned, regrettably elusive are the sole tryptophan and a few other residues in the β-sheet core.

Secondary Structure

Due to their sensitivity to local electronic structure, chemical shifts reflect local conformation. Fig. 9 compares the results of two secondary structure analyses of the chemical shifts of GvpA in *H. salinarum* with the PSIPRED predictions based on primary sequence. The CA-CB analysis [Luca et al., 2001] compares the observed CA and CB chemical shifts for a given residue with the average CA and CB chemical shifts for random coil in existing databases (http://spin.niddk.nih.gov/bax/nmrserver/Poulsen_rc_CS/). TALOS+ [Shen et al., 2009] elaborates by (*i*) adding consideration of the N and CO chemical shifts, (*ii*) also taking into account the shifts of flanking neighbors, and (*iii*) supplementing database mining with neural network processing.

As found earlier for *A. flos-aquae*, the inferences from the experimental data generally agree well with the PSIPRED prediction of an overall

$$\mathrm{coil\,(c1)-helix\,(\alpha 1)-strand\,(\beta 1)-strand\,(\beta 2)-helix\,(\alpha 2)-coil\,(c2)}$$

conformation. Perhaps the most significant discrepancy is that TALOS+ finds the location of the turn between β1 and β2 shifted slightly toward the C-terminus in *H. salinarum*, vs. slightly toward the N-terminus in *A. flos-aquae*. However, the PSIPRED confidence is low in that neighborhood and TALOS is known to have difficulty with “regions of irregular structure, including loops and turns [Shen et al., 2009].

Discussion

In order to confer buoyancy, gas vesicles need to avoid both collapse and condensation of internal water vapor.

Avoiding Water Condensation

Condensation may occur via either homogeneous or heterogeneous nucleation. The former is very slow: for super-saturation levels of 2–4 (as would occur upon cooling by 10 – 20 °C around 300 K), rates of homogeneous water nucleation have been estimated at ~ 1 event per cm^3 per second [Wolk et al., 2002]. Thus, for a typical vesicle, with a volume of less than 10^{-14} cm^3, it would take more than 10^{14} seconds, or about a million years, for homogeneous nucleation to occur. Even for super-saturation levels of 6 (as would occur upon cooling by ~30 °C around 300 K), rates of homogeneous water nucleation rise only to ~10^5 events per cm^3 per second [Wolk et al., 2002], such that nucleation in a volume of less than 10^{-14} cm^3 would take more than 10^9 seconds, still on the order of decades. Thus, all that is required to avoid homogeneous nucleation over relevant time periods is to keep the vesicles small.

Heterogeneous nucleation depends on adsorption at the vesicle surface. For a polar molecule like water, a non-polar surface is less attractive than a polar one. However, even non-polar surfaces, such as carbon nanotubes, can be hospitable to water via dispersive interactions [Hummer et al., 2001; Kyakuno et al., 2011; Maniwa et al., 2002]. These attractions are minimized by an electron poor, i.e., proton rich, composition, as has been observed by x-ray diffraction at the inner surface of gas vesicles [Blaurock and Walsby, 1976]. In this regard, a notable feature of the highly conserved β-strand sequences of GvpA is the presence of an aliphatic residue at every other site. As a result, the β-sheet can present a purely aliphatic face if the β-turn is an odd-membered one. The significance of this constraint will be discussed below.

Avoiding Collapse

As remarked above, it is experimentally observed, as well as commonsensical, that the critical collapse pressures of narrow vesicles are greater than those of wide vesicles. At the same time, more subtle contributions to vesicle strength arise from the numerous hydrogen bonds in the β-sheet. One important feature appears to be antiparallel strand alignment (between, as well as within, monomers) which allows for more regular, and presumably stronger, hydrogen bonds. In addition, hydrogen bonds oriented at the "magic angle" of 54° to the vesicle axis optimally distribute stress [Walsby, 1994]. However this combination is not easily achieved.

In addition to alternating aliphatic residues, another conspicuous feature of the highly conserved sequences of GvpA is the situation of complimentary acidic and basic residues in the non-aliphatic face of β1 at D23---R27 and β2 at E39-R41. These serve to stabilize an antiparallel dimer arrangement, with non-interchangeable pairs of salt-bridges in the β1-β1 and β2-β2 interfaces, such that the bulky helix and coil segments are distributed on both edges of the β-sheet (fig. 10). However, as has previously been noted [Sivertsen et al., 2009], if the dimer is symmetric with the β-turn in both monomers identically centered on the glycine, the hydrogen bonds will be oriented at 70° from the vesicle axis (fig 10a). Alternatively (not shown), if the β-turn in both monomers is identically centered on the neighboring valine (isoleucine), the hydrogen bonds will be oriented at 70° (42°) from the vesicle axis. On the other hand, the "magic angle" is achieved if the β-turn of one monomer is at glycine while the other is at valine (fig. 10b). This dimorphism is consistent with the NMR data for *A. flos-aquae*, both with respect to the duplication of signals [Sivertsen et al., 2009] and with respect to distances between residues in the β1-β1 and β2-β2 interfaces [Bayro et al., 2012]. However, the advantage of the "magic angle" appears to have been foregone in *H. salinarum*, since the NMR shows no evidence of dimorphism.

Trade-offs

The picture that emerges is that, while *H. salinarum* and *A. flos-aquae* appear to adopt similar strategies with regard to preventing condensation of water vapor inside their gas vesicles, *H. salinarum*, inhabiting shallow brine pools, appears to be able to economize on vesicle strength in ways that *A. flos-aquae*, inhabiting deep fresh water lakes, does not. The evidence available suggests that both species form β-sheets with one purely aliphatic face. If this face presents to the vesicle interior, it will minimize heterogeneous nucleation of water. The two species also keep their internal volumes small, which has the effect of minimizing homogeneous nucleation of water. However, the rounder *H. salinarum* vesicles achieve volumes comparable to those of the longer and narrower *A. flos-aquae* vesicles with a smaller surface area and a correspondingly smaller investment in the protein shell. *H. salinarum* also appears to economize by making use of a single, presumably lowest energy, monomer conformation and making do with the resulting suboptimal orientation of the hydrogen bonds. It seems likely that these differences have more to do with adaptation to habitat than with the evolutionary divergence between bacteria and archaea. It would be interesting to carry out studies of wide bacterial gas vesicles and narrow archaeal gas vesicles.

Experimental Procedures

H. salinarum gas vesicles were prepared as described previously [Belenky et al., 2004] except that the *H. salinarum* cells were grown on a uniformly ^{13}C,^{15}N-labeled medium. The isolated ^{13}C,^{15}N-labeled gas vesicles were collapsed by a pressure pulse, washed and then centrifuged into Bruker 3.2 zirconia mm rotors following the protocol applied previously to previously *A. flos-aquae* vesicles [Sivertsen et al., 2009].

One-dimensional ^{13}C spectra (fig. 4) were acquired at 750 MHz ^{1}H Larmor frequency and 16 kHz MAS. The cross-polarization (CP) [Metz et al., 1994; Pines et al., 1972] and direct-polarization spectra are the averages of 512 scans each, whereas the spectrum from insensitive nuclei enhanced by polarization transfer (INEPT) [Morris and Freeman, 1979] is the average of 1600 scans.

The two-dimensional ^{15}N-^{13}C ZF-TEDOR [Jaroniec et al., 2002] spectrum (fig. 5) was obtained at 900 MHz ^{1}H Larmor frequency and 16.6 kHz MAS, using a triple-resonance 3.2 mm $^{1}H/^{13}C/^{15}N$ E-free probe (Bruker Biospin, Billerica, MA). The mixing period was optimized for one bond transfers at 1.4 ms, and 83 kHz two-pulse phase modulation (TPPM) decoupling [Bennett et al., 1995] was applied during the evolution and detection periods. The spectrum was recorded with 250 real and 250 imaginary points in the indirect dimension and 4096 points in the direct dimension, with dwell times of 60 μs and 6 μs, respectively. The spectra are the average of 128 transients per t_1 point.

Two-dimensional ^{13}C-^{13}C spectra (fig. 6) were acquired at 750 MHz ^{1}H Larmor frequency and 16 kHz MAS. The radio-frequency-driven dipolar recoupling (RFDR) [Bayro et al., 2008; Bennett et al., 1992; Bennett et al., 1998] mixing time was optimized for one bond transfers at 2 ms. The dipolar assisted rotational resonance (DARR) [Takegoshi et al., 2001; Veshtort and Griffin, 2011] mixing time was optimized for one-to-two bond at 10 ms. Both experiments made use of 83 kHz two-pulse phase modulation (TPPM) decoupling [Bennett et al., 1995] during the evolution and detection periods. Both experiments were recorded with 500 real and 500 imaginary points in the indirect dimension and 1536 points in the direct dimension, with dwell times of 20 ms and 14 ms, respectively. The spectra are the average of 48 transients per t_1 point.

The three-dimensional ^{15}N-^{13}C-^{13}C spectra (fig. 7) were acquired at 750 MHz ^{1}H Larmor frequency and 16±2 kHz MAS using a triple-resonance 3.2 mm $^{1}H/^{13}C/^{15}N$ E-free probe (Bruker Biospin, Billerica, MA). The 90° ^{15}N and ^{13}C pulses were 5 ms and 2.5 ms, respectively. TPPM decoupling was 83 kHz during the gaps between REDOR pulses and acquisition, and 100 kHz during evolution. Mixing periods were 1.5 ms for ZF-TEDOR and 40 ms for DARR, the latter chosen to transfer polarization into the protein side-chains. The 3D data set was acquired using 60 × 220 × 896 points, with dwell times of 125, 34 and 20 μs, for ω_1, ω_2 and ω_3 respectively. Each FID averaged four scans, using a recycle delay of 2.6 s, for a total experimental time of 6.3 days.

All spectra were referenced to external 2,2-dimethyl-2-silapentane-5-sulfonic acid [Morcombe and Zilm, 2003].

All data sets were processed with the NMRPipe package [Delaglio et al., 1995] and analyzed using Sparky (Goddard, T. D. and D. G. Kneller. SPARKY 3. University of California, San Francisco).

Acknowledgments

Research reported in this publication was supported by the National Institute of. Biomedical Imaging and Bioengineering of the National Institutes of Health under awards EB001035, EB001960 and EB002026. The content is solely the responsibility of the authors and does not necessarily represent the official views of the National Institutes of Health.

References

Bayro MJ, Daviso E, Belenky M, Griffin RG, Herzfeld J. An amyloid organelle, solid-state nmr evidence for cross-beta assembly of gas vesicles. Journal of Biological Chemistry. 2012; 287:3479–3484. [PubMed: 22147705]

Bayro MJ, Ramachandran R, Caporini MA, Eddy MT, Griffin RG. Radio frequency-driven recoupling at high magic-angle spinning frequencies: Homonuclear recoupling sans heteronuclear decoupling. Journal of Chemical Physics. 2008; 128:052321–052311. [PubMed: 18266438]

Belenky M, Meyers R, Herzfeld J. Subunit structure of gas vesicles: A maldi-tof mass spectrometry study. Biophysical Journal. 2004; 86:499–505. [PubMed: 14695294]

Bennett AE, Ok JH, Griffin RG, Vega S. Chemical shift correlation spectroscopy in rotating solids - radio frequency-driven dipolar recoupling and longitudinal exchange. J Chem Phys. 1992; 96:8624–8627.

Bennett AE, Rienstra CM, Auger M, Lakshmi KV, Griffin RG. Heteronuclear decoupling in rotating solids. Journal of Chemical Physics. 1995; 103:6951–6958.

Bennett AE, Rienstra CM, Griffiths JM, Zhen WG, Lansbury PT, Griffin RG. Homonuclear radio frequency-driven recoupling in rotating solids. Journal of Chemical Physics. 1998; 108:9463–9479.

Blaurock AE, Walsby AE. Crystalline structure of gas vesicle wall from anabaena-flos-aquae. Journal of Molecular Biology. 1976; 105:183–199. [PubMed: 184286]

Blaurock AE, Wober W. Structure of the wall of *halobacterium halobium* gas vesicles. Journal of Molecular Biology. 1976; 106:871–888. [PubMed: 978738]

Daviso E, Eddy MT, Andreas LB, Griffin RG, Herzfeld J. Efficient resonance assignment of proteins in mas nmr by simultaneous intra- and inter-residue 3d correlation spectroscopy. Journal of Biomolecular NMR. 2013 in press.

Delaglio F, Grzesiek S, Vuister GW, Zhu G, Pfeifer J, Bax A. Nmrpipe - a multidimensional spectral processing system based on unix pipes. J Biomol NMR. 1995; 6:277–293. [PubMed: 8520220]

Ezzeldin HM, Klauda JB, Solares SD. Modeling of the major gas vesicle protein, gvpa: From protein sequence to vesicle wall structure. J Struct Biol. 2012; 179:18–28. [PubMed: 22580065]

Hummer G, Rasaiah JC, Noworyta JP. Water conduction through the hydrophobic channel of a carbon nanotube. Nature. 2001; 414:188–190. [PubMed: 11700553]

Jaroniec CP, Filip C, Griffin RG. 3d tedor nmr experiments for the simultaneous measurement of multiple carbon-nitrogen distances in uniformly c-13, n-15-labeled solids. Journal of the American Chemical Society. 2002; 124:10728–10742. [PubMed: 12207528]

Kyakuno H, Matsuda K, Yahiro H, Inami Y, Fukuoka T, Miyata Y, Yanagi K, Maniwa Y, Kataura H, Saito T, Yumura M, Iijima S. Confined water inside single-walled carbon nanotubes: Global phase diagram and effect of finite length. Journal of Chemical Physics. 2011:134.

Luca S, Filippov DV, van Boom JH, Oschkinat H, de Groot HJM, Baldus M. Secondary chemical shifts in immobilized peptides and proteins: A qualitative basis for structure refinement under magic angle spinning. J Biomol NMR. 2001; 20:325–331. [PubMed: 11563556]

Maniwa Y, Kataura H, Abe M, Suzuki S, Achiba Y, Kira H, Matsuda K. Phase transition in confined water inside carbon nanotubes. Journal of the Physical Society of Japan. 2002; 71:2863–2866.

McMaster TJ, Miles MJ, Walsby AE. Direct observation of protein secondary structure in gas vesicles by atomic force microscopy. Biophysical Journal. 1996; 70:2432–2436. [PubMed: 9172769]

Metz G, Wu XL, Smith SO. Ramped amplitude cross-polarization in magic-angle-spinning nmr. Journal of Magnetic Resonance Series A. 1994; 110:219–227.

Morcombe CR, Zilm KW. Chemical shift referencing in mas solid state nmr. Journal of Magnetic Resonance. 2003; 162:479–486. [PubMed: 12810033]

Morris GA, Freeman R. Enhancement of nuclear magnetic-resonance signals by polarization transfer. J Am Chem Soc. 1979; 101:760–762.

Offner S, Ziese U, Wanner G, Typke D, Pfeifer F. Structural characteristics of halobacterial gas vesicles. Microbiology-Sgm. 1998; 144:1331–1342.

Omelchenko MV, Vasilyeva LV, Zavarzin GA. Psychrophilic methanotroph from tundra soil. Current Microbiology. 1993; 27:255–259.

Pines A, Waugh JS, Gibby MG. Proton-enhanced nuclear induction spectroscopy - method for high resolution nmr of dilute spins in solids. Journal of Chemical Physics. 1972; 56:1776–1777.

Ramsay JP, Williamson NR, Spring DR, Salmond GPC. A quorum-sensing molecule acts as a morphogen controlling gas vesicle organelle biogenesis and adaptive flotation in an

enterobacterium. Proceedings of the National Academy of Sciences of the United States of America. 2011; 108:14932–14937. [PubMed: 21873216]

Shen Y, Delaglio F, Cornilescu G, Bax A. Talos+: A hybrid method for predicting protein backbone torsion angles from nmr chemical shifts. Journal of Biomolecular NMR. 2009; 44:213–223. [PubMed: 19548092]

Sivertsen AC, Bayro MJ, Belenky M, Griffin RG, Herzfeld J. Solid-state nmr evidence for inequivalent gvpa subunits in gas vesicles. Journal of Molecular Biology. 2009; 387:1032–1039. [PubMed: 19232353]

Sivertsen AC, Bayro MJ, Belenky M, Griffin RG, Herzfeld J. Solid-state nmr characterization of gas vesicle structure. Biophysical Journal. 2010; 99:1932–1939. [PubMed: 20858439]

Strunk T, Hamacher K, Hoffgaard F, Engelhardt H, Zillig MD, Faist K, Wenzel W, Pfeifer F. Structural model of the gas vesicle protein gvpa and analysis of gvpa mutants in vivo. Molecular Microbiology. 2011; 81:56–68. [PubMed: 21542854]

Takegoshi K, Nakamura S, Terao T. C13-h1 dipolar-assisted rotational resonance in magic-angle spinning nmr. Chem Phys Lett. 2001; 344:631–637.

Veshtort M, Griffin RG. Proton-driven spin diffusion in rotating solids via reversible and irreversible quantum dynamics. Journal of Chemical Physics. 2011; 135:134509. [PubMed: 21992326]

Walker JE, Hayes PK, Walsby AE. Homology of gas vesicle proteins in cyanobacteria and halobacteria. Journal of General Microbiology. 1984; 130:2709–2715.

Walsby AE. Permeability of blue-green algal gas-vacuole membranes to gas. Proceedings of the Royal Society of London Series B-Biological Sciences. 1969; 173:235–255.

Walsby AE. Permeability of gas vesicles to perfluorocyclobutane. Journal of General Microbiology. 1982; 128:1679–1684.

Walsby AE. Gas vesicles. Microbiological Reviews. 1994; 58:94–144. [PubMed: 8177173]

Walsby AE, Hayes PK. The minor cyanobacterial gas vesicle protein, gvpc, is attached to the outer surface of the gas vesicle. Journal of General Microbiology. 1988; 134:2647– 2657.

Walsby AE, Revsbech NP, Griffel DH. The gas-permeability coefficient of the cyanobacterial gas vesicle wall. Journal of General Microbiology. 1992; 138:837–845.

Walsby AE, Simpson JH. Lower limit of the gas-permeability coefficient of gas vesicles. Proceedings of the Royal Society of London Series B-Biological Sciences. 1984; 223:177.

Wolk J, Strey R, Heath CH, Wyslouzil BE. Empirical function for homogeneous water nucleation rates. Journal of Chemical Physics. 2002; 117:4954–4960.

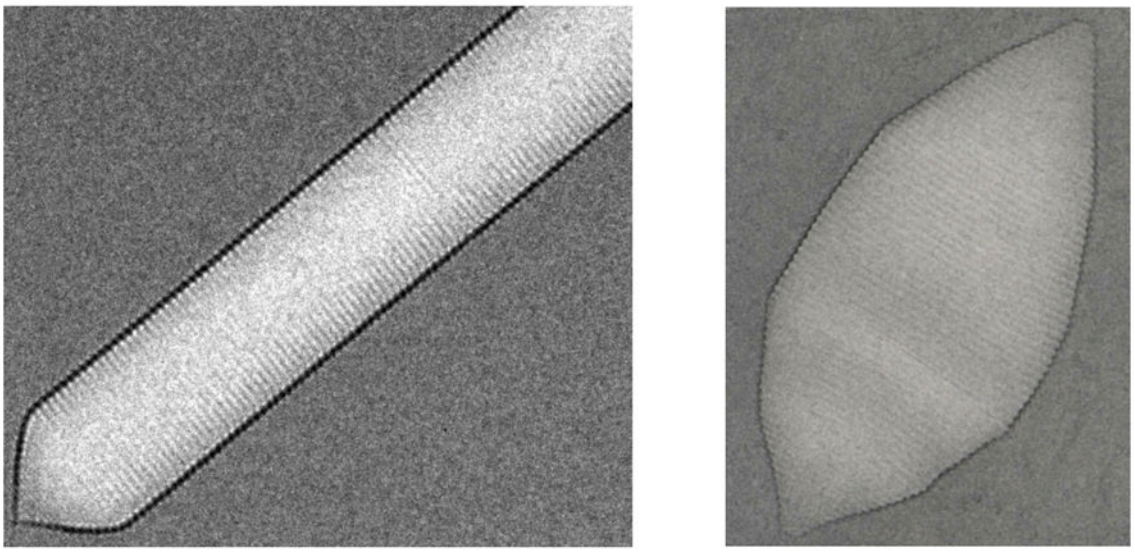

Fig. 1.
Electron micrographs of gas vesicles from *Anabaena flos-aquae* (left, obtained in collaboration with Chen Xu, Brandeis University) and *Halobacterium salinarum* (right, obtained in collaboration with L. A. Melanson and D. DeRosier, Brandeis University) scaled to approximately match the 46 Å spacings of their ribs. On closer examination of the images, a bipolar structure is evident from the opposite orientations of the rib protrusions on either side of an apparent seam.

Fig. 2.

Primary sequences of GvpA in the cyanobacterium *Anabaena flos-aquae* (top) and in the haloarchaea *Halobacterium salinarum* (middle pair), and *Haloferax mediterranei* (bottom). Substitutions in the unshaded, central region are few and highly conservative. Non-conservative variations in the shaded, peripheral regions add considerable negative charge to the halophile proteins.

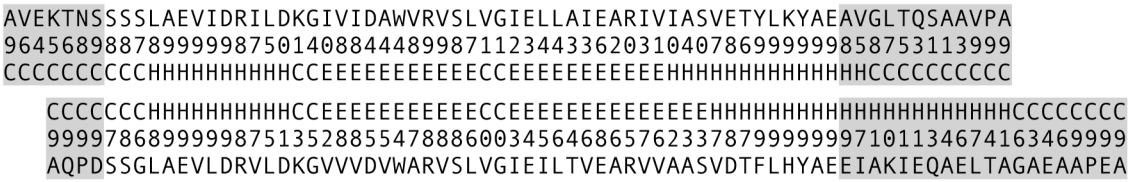

Fig. 3.

Secondary structure predictions from PSIPRED v3.0 for the GvpA of *Anabaena flos-aquae* (top) and in the dominant GvpA of *Halobacterium salinarum* (bottom). Shading as in Figure 2. Notation: C=coil, H=helix, E=strand, with confidence ranging from 0 (low) to 9 (high). In both cases, all the glycine residues are found near transitions between secondary conformations.

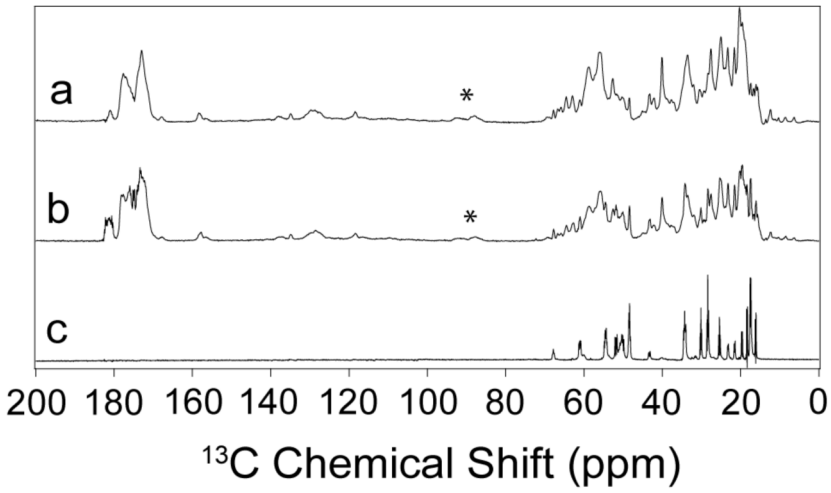

Fig. 4.

MAS NMR spectra of gas vesicles of *H. salinarum* at approximately 3°C using (a) cross-polarization, (b) direct polarization, and (c) ^{1}H-^{13}C INEPT. The asterisks identify spinning sidebands.

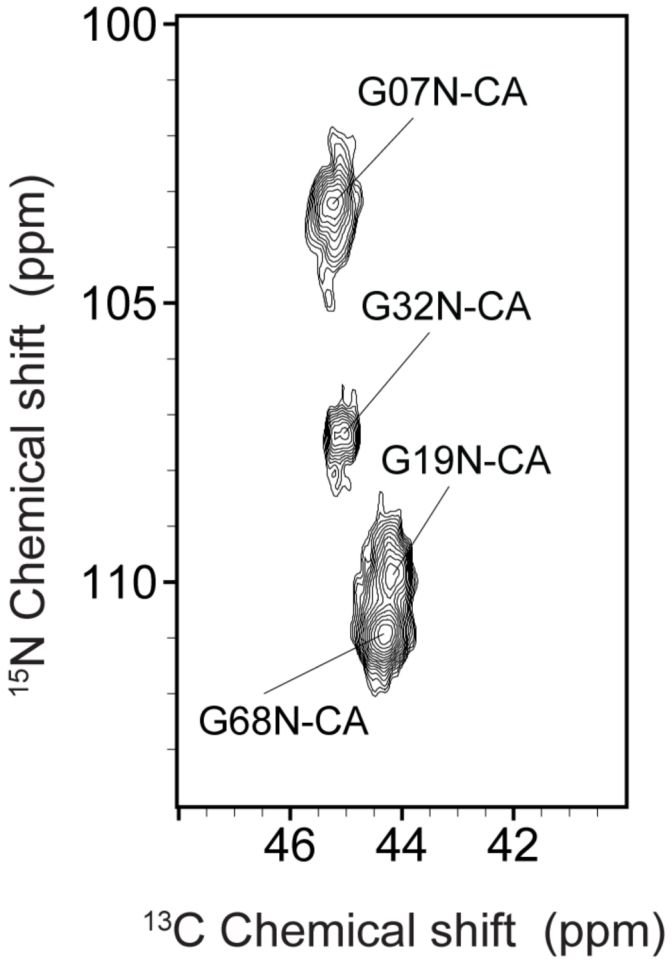

Fig. 5.
N-CA correlations in the glycine region observed at 900 MHz ^{1}H Larmor frequency and 3°C, using 1.4 ms of ZF-TEDOR mixing. Signals were assigned as described in the text.

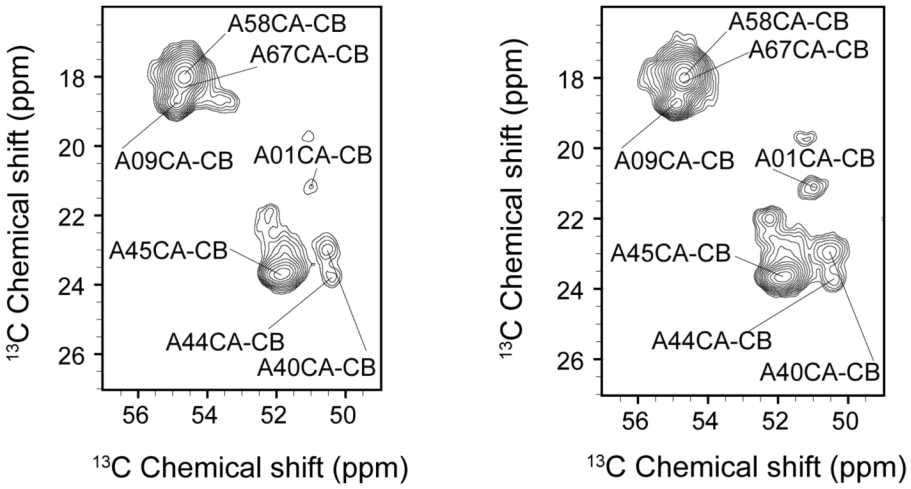

Fig. 6.

CA-CB correlations in the alanine region observed at 750 MHz ^{1}H Larmor frequency and 3°C, using 2 ms of RFDR mixing (left) or 10 ms of DARR mixing (right). Although the two methods differ in polarization transfer characteristics and not all of the peaks have been assigned (see text), the two spectra taken together do not make a case for more than 14 distinct alanine signals.

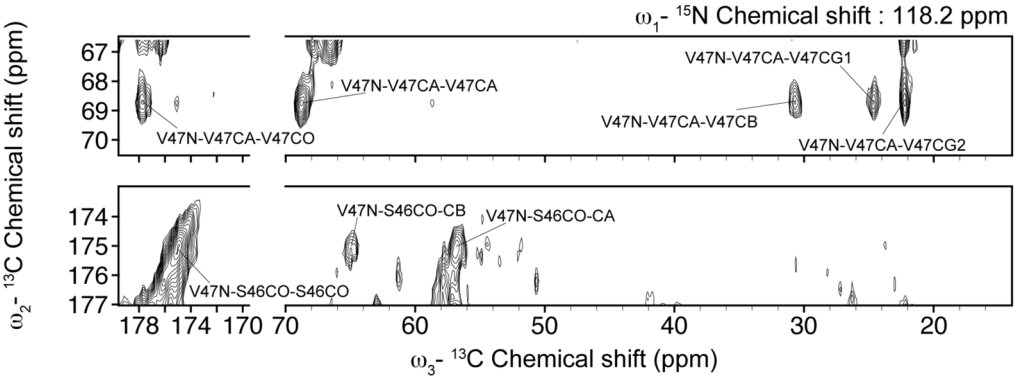

Fig. 7.

Slices of the ZF-TEDOR-DARR ^{15}N-^{13}C-^{13}C spectrum at 750 MHz ^{1}H Larmor frequency and 3°C showing NCaCx correlations (top) and NCOCx correlations (bottom) at the ^{15}N frequency of the V47 amides.

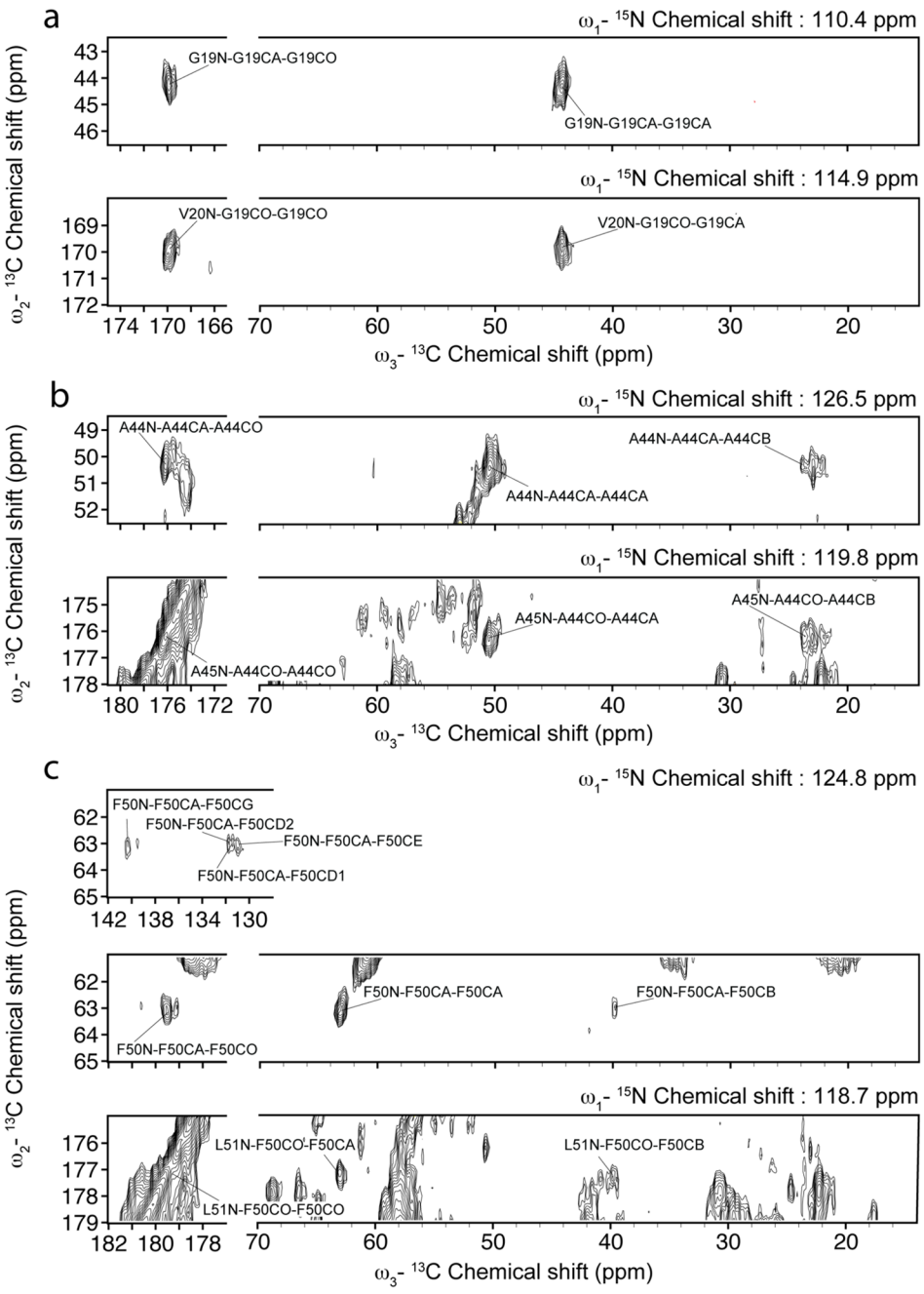

Fig. 8.

Slices of the ZF-TEDOR-DARR ^{15}N-^{13}C-^{13}C spectrum at 750 MHz ^{1}H Larmor frequency and 3°C showing,

(a) NCACX correlations (top) and NCOCX correlations (bottom) at the ^{15}N frequencies of the G19 amide (top) and of the V20 amide (bottom),

(b) NCACX correlations (top) and NCOCX correlations (bottom) at the ^{15}N frequencies of the A44 amide (top) and of the A45 amide (bottom), and

(c) NCACX correlations (top) and NCOCX correlations (bottom) at the ^{15}N frequencies of the F50 amide (top) and of the L51 amide (bottom).

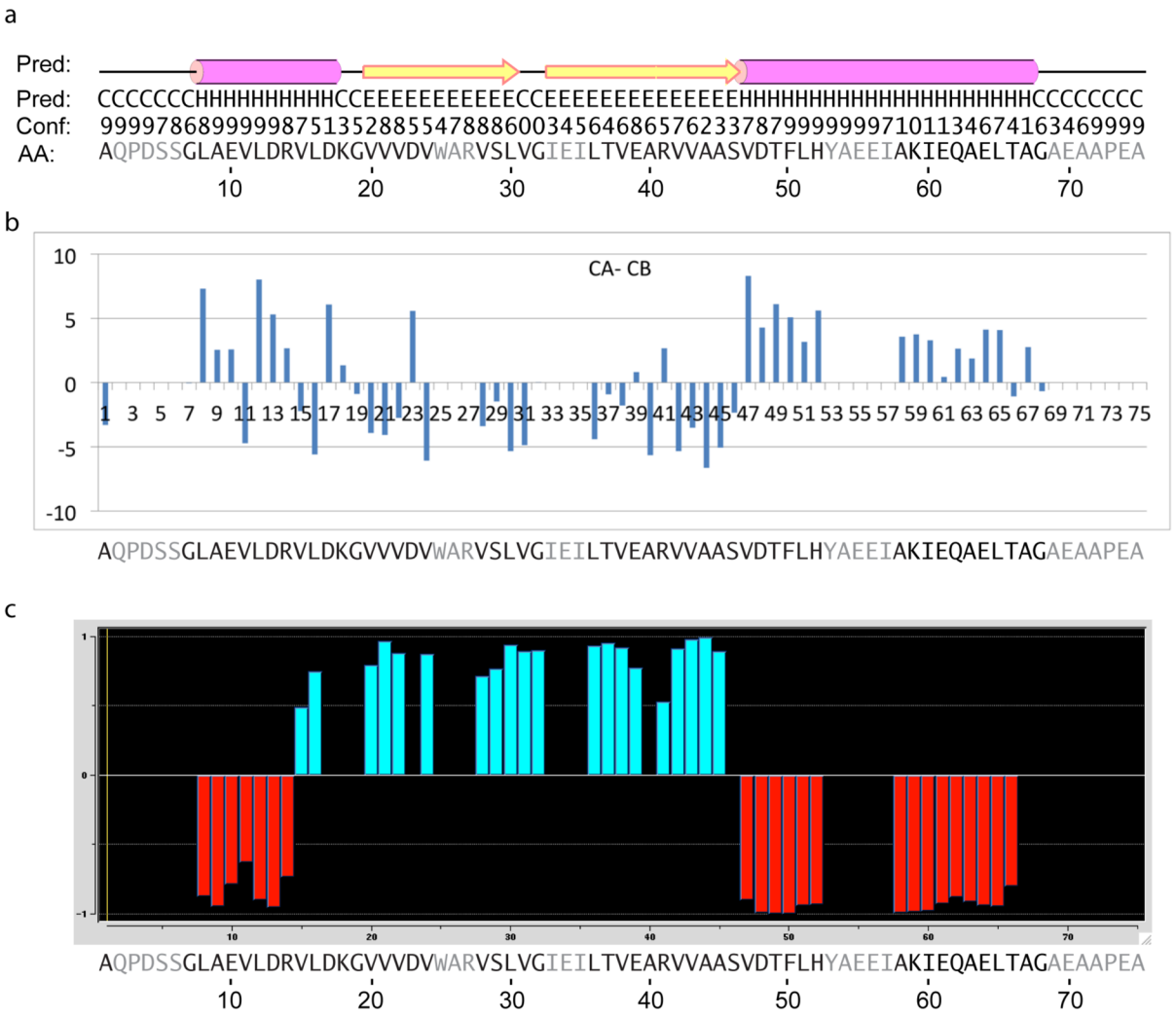

Fig. 9.

Secondary structure results for GvpA in *H. salinarum*. In all panels, the amino acid residues that remain unassigned are shaded in gray.

(a) Repeat of the PSIPRED prediction shown in fig. 3.

(b) Results of CA-CB analysis. Positive and negative values identify helix and strand conformations, respectively.

(c) Results of TALOS+ analysis. Negative and positive values identify helix and strand conformations, respectively.

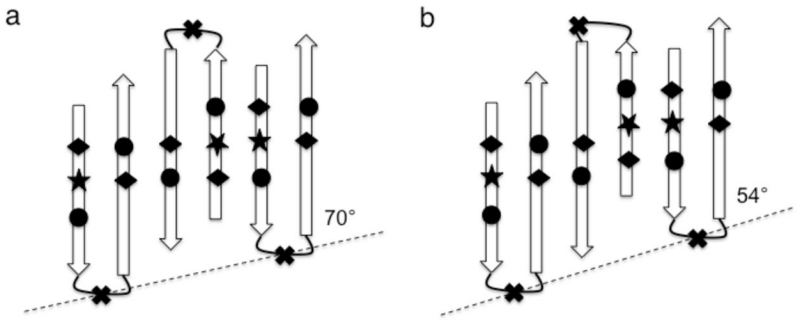

Fig. 10.

Schematic representation of two ways of forming an extended, anti-parallel β-sheet along the vesicle rib (dashed lines), employing antiparallel dimers that distribute the helix and coil segments of GvpA on both edges of the sheet. All β-turns are odd-membered so that all the non-aliphatic residues, including the unique tryptophan (★), are on the side of the sheet facing the reader and all charged residues [carboxylic acids (♦) and arginines (●)] are paired in salt bridges. (a) With a symmetric dimer unit cell in which both β-turns are centered on glycine (✖), the inclinations of the strands to the rib and the hydrogen bonds to the vesicle axis are 70°. (b) with an asymmetric dimer unit cell, in which β-turns in alternating molecules are centered on valine instead of glycine, the inclinations of the strands to the rib and the hydrogen bonds to the vesicle axis are 54°. Note that the angles do not appear to be of the labeled magnitude because the distances between strands have been rendered on a larger scale than the distances along strands in order to enhance clarity.